AD_____

Award Number: DAMD17-01-1-0226

TITLE: New Approaches in SPECT Breast Imaging

PRINCIPAL INVESTIGATOR: Brett Pieper
R. Jaszczak, Ph.D.
M. Tornai, Ph.D.
J. Bowsher, Ph.D.

CONTRACTING ORGANIZATION: Duke University
Durham, North Carolina 27708-0077

REPORT DATE: July 2002

TYPE OF REPORT: Annual Summary

PREPARED FOR: U.S. Army Medical Research and Materiel Command
Fort Detrick, Maryland 21702-5012

REPORT DOCUMENTATION PAGE

Form Approved
OMB No. 074-0188

1. AGENCY USE ONLY (Leave blank)	2. REPORT DATE	3. REPORT TYPE AND DATES COVERED
	July 2002	Annual Summary (1 Jul 01 - 30 Jun 02)

4. TITLE AND SUBTITLE
New Approaches in SPECT Breast Imaging

5. FUNDING NUMBERS
DAMD17-01-1-0226

6. AUTHOR(S):
Brett Pieper, R. Jaszczak, Ph.D., M. Tornai, Ph.D., J. Bowsher, Ph.D.

7. PERFORMING ORGANIZATION NAME(S) AND ADDRESS(ES)
Duke University
Durham, North Carolina 27708-0077

E-Mail: pieper@dec3.mc.duke.edu

8. PERFORMING ORGANIZATION REPORT NUMBER

9. SPONSORING / MONITORING AGENCY NAME(S) AND ADDRESS(ES)
U.S. Army Medical Research and Materiel Command
Fort Detrick, Maryland 21702-5012

10. SPONSORING / MONITORING AGENCY REPORT NUMBER

11. SUPPLEMENTARY NOTES

12a. DISTRIBUTION / AVAILABILITY STATEMENT
Approved for Public Release; Distribution Unlimited

12b. DISTRIBUTION CODE

13. Abstract ***(Maximum 200 Words)*** *(abstract should contain no proprietary or confidential information)*
Parallel-beam Tilted-Head SPECT (TH-SPECT) was implemented on a SPECT system for its potential to image breast lesions and nearby axilla of seated, upright women. Breast, liver, and myocardial activity were included in order to simulate direct contamination and Compton scattering expected in clinical scans. Results indicated an increase in axial blurring with greater tilt angle. Reconstructions of combined fillable breast and torso phantoms containing two 1.15 ml lesions were most clearly visible in the 30° reconstructed TH-SPECT images, providing lesion SNR and contrast improvements of nearly three times compared to the high-count planar images Because it is not clear which reconstruction method, if any, is better suited for TH-SPECT data, a geometric derivation of the ramp filter for tilted parallel-beam geometries was explored. A filtered backprojection (FBP) algorithm, using this filter, was then implemented and compared with an iterative Ordered Subsets Expectation Maximization (OSEM) algorithm, using TH-SPECT data. Results indicated OSEM SNR and contrast values were higher at all degrees of tilt and may offer better shape and uniform activity distribution of the breast compared to FBP methods.

14. SUBJECT TERMS	15. NUMBER OF PAGES
nuclear medicine, SPECT (single photon emission computed tomography), filtered backprojection	19
	16. PRICE CODE

17. SECURITY CLASSIFICATION OF REPORT	18. SECURITY CLASSIFICATION OF THIS PAGE	19. SECURITY CLASSIFICATION OF ABSTRACT	20. LIMITATION OF ABSTRACT
Unclassified	Unclassified	Unclassified	Unlimited

Table of Contents

Introduction

The primary objective of this work is to develop new techniques in single photon emission computed tomography (SPECT) breast cancer imaging providing improved detection and characterization of early stage breast cancer. Conventional SPECT breast imaging uses a horizontal axis of rotation and thus requires a large radius of rotation. By using a vertical axis of rotation (VAOR) and various camera head and collimator configurations, the effective radius of rotation (ROR) can be reduced and background myocardial and liver interference can be minimized. A tiltable head SPECT (TH-SPECT) system with a VAOR further allows for improved imaging of lesions near the chest wall and reduction of effective ROR [2]. Investigation of new reconstruction algorithms for the TH-SPECT geometry is then needed to accurately (and efficiently) reconstruct TH-SPECT data [1]. This research investigates the feasibility of TH-SPECT acquisition and reconstruction.

Body (outlined with *Statement of Work*)

Task 1. Develop TH-SPECT image reconstruction algorithm

Refer to attached:

[1] BC Pieper, JE Bowsher, MP Tornai, J Peter, CN Archer, RJ Jaszczak. "Parallel-beam Tilted-head Analytic SPECT Reconstruction." IEEE Transactions on Nuclear Science, in press, 2002

Task 2. Investigate various VAOR system configurations as well has different camera head geometries and collimator configurations.

Refer to attached:

[2] BC Pieper, JE Bowsher, MP Tornai, J Peter, RJ Jaszczak. "Breast Tumor Imaging Using Tiltable Head SPECT Cameras." IEEE Transactions on Nuclear Science, vol. 48, no. 4. pp 1477-1482, 2001.

Key Research Accomplishments

- Development and evaluation of FBP TH-SPECT image reconstruction algorithm [1].
- Comparison of FBP TH-SPECT algorithm with traditional FBP and OSEM reconstruction methods [1].
- Acquisition, evaluation, and comparison of TH-SPECT data, including contrast and S/N analysis using experimental phantoms [2].

Reportable Outcomes

[1] BC Pieper, JE Bowsher, MP Tornai, J Peter, CN Archer, RJ Jaszczak. "Parallel-beam Tilted-head Analytic SPECT Reconstruction." IEEE Transactions on Nuclear Science, in press, 2002

[2] BC Pieper, JE Bowsher, MP Tornai, J Peter, RJ Jaszczak. "Breast Tumor Imaging Using Tiltable Head SPECT Cameras." IEEE Transactions on Nuclear Science, vol. 48, no. 4. pp 1477-1482, 2001.

Brett Pieper, Master of Science, Biomedical Engineering, Duke University, May 2002

Conclusions

TH-SPECT is an exciting new technique in SPECT breast cancer imaging. Focus on TH-SPECT feasibility, especially with small field-of-view SPECT cameras, as well as improved reconstruction methods may someday supplant traditional breast cancer detection methods. Initial results of this research have indicated the advantages of TH-SPECT and successful TH-SPECT (analytic and iterative) reconstruction. Further research, particularly patient studies, will be required to realize the full potential of TH-SPECT breast cancer imaging.

References

[1] BC Pieper, JE Bowsher, MP Tornai, J Peter, CN Archer, RJ Jaszczak. "Parallel-beam Tilted-head Analytic SPECT Reconstruction." IEEE Transactions on Nuclear Science, in press, 2002

[2] BC Pieper, JE Bowsher, MP Tornai, J Peter, RJ Jaszczak. "Breast Tumor Imaging Using Tiltable Head SPECT Cameras." IEEE Transactions on Nuclear Science, vol. 48, no. 4. pp 1477-1482, 2001.

Appendices

[1] BC Pieper, JE Bowsher, MP Tornai, J Peter, CN Archer, RJ Jaszczak. "Parallel-beam Tilted-head Analytic SPECT Reconstruction." IEEE Transactions on Nuclear Science, in press, 2002

[2] BC Pieper, JE Bowsher, MP Tornai, J Peter, RJ Jaszczak. "Breast Tumor Imaging Using Tiltable Head SPECT Cameras." IEEE Transactions on Nuclear Science, vol. 48, no. 4. pp 1477-1482, 2001.

Parallel-beam Tilted-head Analytic SPECT Reconstruction: Derivation and Comparison with OSEM

Brett C. Pieper, *Member, IEEE*, James E. Bowsher, *Member, IEEE*, Martin P. Tornai, *Member, IEEE*, Caryl N. Archer, *Member, IEEE*, Ronald J. Jaszczak, *Fellow, IEEE*

Abstract— **Parallel-beam Tilted-Head SPECT (TH-SPECT) was previously implemented on a SPECT system for its potential to image breast lesions and nearby axilla of seated, upright women. All TH-SPECT reconstructions will contain artifacts since the tilted orbit does not satisfy the Orlov sampling criteria. However, it is not clear which reconstruction method, if any, is better suited for TH-SPECT data. Here a geometric derivation of the ramp filter for tilted parallel-beam geometries is presented. A filtered backprojection (FBP) algorithm, using this filter, was then implemented and compared with an iterative Ordered Subsets Expectation Maximization (OSEM) algorithm, using TH-SPECT data. A breast scan at various tilt angles was simulated and used to generate a noise vs. bias study for both methods. Contrast and SNR values as well as axial elongation present in all TH-SPECT reconstructions were characterized using a mini-Defrise disk phantom placed inside a fillable breast phantom and imaged from 0-15 degree head tilt. A fillable breast phantom containing lesions was also imaged with a system dedicated to prone breast SPECT from 0-30 degrees to evaluate the effects of incomplete sampling due to greater tilt angles. FBP noise vs. bias studies indicated a greater increase in bias with tilt angle compared to OSEM reconstructions. At small tilt angles about the mini-Defrise disk phantom, poorer contrasts were obtained with FBP compared to OSEM at similar noise levels. All reconstructions of the fillable breast phantom indicated axial elongation at greater tilt angles, although FBP reconstructions displayed an increase in stretching distortions of the breast. OSEM SNR and contrast values were higher at all degrees of tilt. In conclusion, measured results indicate OSEM TH-SPECT reconstruction provides better contrast and SNR values and may offer better shape and uniform activity distribution of the breast compared to FBP methods.**

I. Introduction

Tilted-Head Single Photon Emission Computed Tomography (TH-SPECT) parallel-beam imaging of breast lesions has been shown to offer superior lesion contrast and signal-to-noise ratio (SNR) values compared to conventional SPECT geometries [1]. Reconstruction of TH-SPECT data requires a three-dimensional reconstruction algorithm. Iterative methods have thus far been used to accurately model the complex (albeit incomplete) sampling of frequency space associated with the tilted circular orbit. It may be useful, however, to reconstruct TH-SPECT data using analytic filtered backprojection (FBP) methods given the speed and linearity associated with such methods.

Manuscript received November 5, 2001. This work was funded by grant DAMD17-01-1-0226 from the Department of Defense, PHS grants R01-CA76006 and R01-CA33541 from the National Institutes of Health, grant RG-99-0305 from the Whitaker Foundation, and grant DE-FG02-96ER62150 from the Department of Energy.

B.C. Pieper, M. P. Tornai, C.N. Archer, and R. J. Jaszczak are with the Department of Biomedical Engineering, Duke University and the Department of Radiology, Duke University Medical Center. J. E. Bowsher is with the Department of Radiology, Duke University Medical Center, Durham, NC 27710 USA (telephone: 919-684-7687, 919-684-7788, 919-684-7791, 919-684-7766, 919-684-7785, e-mail: pieper@dec3.mc.duke.edu, jeb@dec3.mc.duke.edu, martin.tornai@duke.edu, cnb3@duke.edu, rjj@dec3.mc.duke.edu).

Conventional 2-D FBP SPECT reconstruction for parallel-beam collimation relies on the standard one-dimensional ramp filter. This ramp filter has also been shown to be the backprojection filter for 3-D tilted parallel-beam geometries [2]. Due to insufficient Orlov Sphere sampling [3], TH-SPECT acquisitions introduce a null space of unmeasured frequency components whose frequency-space volume is dependent upon tilt angle. These unmeasured frequency components may have negative effects on image reconstruction. One such effect is axial stretching which produces unwanted distortion of the patient's body contour [1]. Another related effect is inaccurate activity distribution specifically due to insufficient sampling of the Orlov Sphere. With these negative effects in mind, it is unclear which image reconstruction method is better suited for TH-SPECT data. This paper develops a geometric derivation of the ramp filter for TH-SPECT and then compares parallel-beam TH-SPECT FBP reconstruction with an existing iterative Ordered Subsets Expectation Maximization (OSEM) algorithm [1], [4]. Simulation studies as well as phantom studies are performed and evaluated.

II. Methods

A. TH-SPECT reconstruction

Three spatial domain coordinate systems are used (Fig. 1) and are defined as (x,y,z), (x',y',z'), and (x'',y'',z''). The object is expressed within the fixed (x,y,z) coordinate system as $f(x,y,z)$. The (x',y',z') system is a rotational coordinate system rotated about the z axis by angle θ. The third coordinate system (x'',y'',z'') represents the tilt of the (x',y',z') system about the y' axis by tilt angle ϕ. The object's frequency domain representation is expressed within the fixed (μ,ν,τ) system as $F(\mu,\nu,\tau)$, and rotations within this system are similarly defined as (μ',ν',τ'), and (μ'',ν'',τ'').

Rotation of (x,y,z), or similarly (μ,ν,τ), by angle θ produces the following transformations

$$\begin{aligned} x' &= x\cos\theta + y\sin\theta \\ y' &= -x\sin\theta + y\cos\theta \\ z' &= z. \end{aligned} \tag{1}$$

Likewise, rotation of (x',y',z'), or similarly (μ',ν',τ'), by angle ϕ produces the following transformations

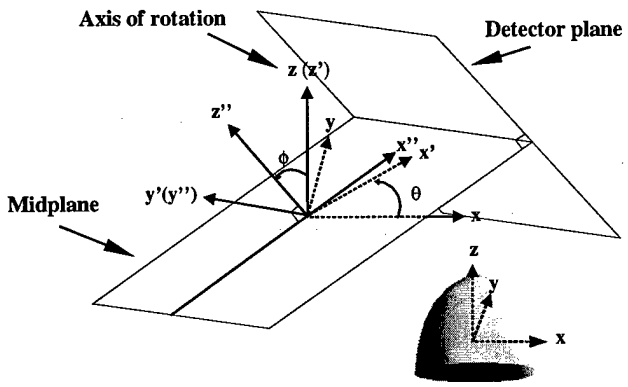

Fig. 1. Illustration of tilted geometry and (x,y,z) coordinate system. Lower-right illustration indicates breast positioning within the tilted geometry, where the z axis passes through the nipple and the center of the base of the breast. Dashed lines indicate axis is behind object.

$$\begin{aligned} x'' &= x\cos\theta\cos\phi + y\sin\theta\cos\phi - z\sin\phi \\ y'' &= -x\sin\theta + y\cos\theta \\ z'' &= x\cos\theta\sin\phi + y\sin\theta\sin\phi + z\cos\phi. \end{aligned} \tag{2}$$

A.1 Backprojection filter for non-tilted parallel-beam geometry

In order to suggest a filter for TH-SPECT data, we first examine filtering for non-tilted parallel-beam geometries. The Fourier projection-slice theorem implies that by taking projections at multiple angles θ with $\phi = 0$, values of $F(\mu,\nu,\tau)$ will be known along radial planes centered at the origin and perpendicular to the projections [5], [6], [7], [8], [9], [10]. Figure 2 (top) illustrates the frequency domain representation of a single non-tilted projection at angle θ, with ω being the distance from one arbitrary sample point to the axis of rotation (AOR) τ. Rotation about τ fills $F(\mu,\nu,\tau)$ with multiple circles of discrete sample points. Figure 2 (bottom) illustrates a slice at a constant value of τ. As the radial distance ω increases, the density of sample points within a given rotation circle decreases. Specifically, the density of sample points within each circle is directly proportional to $\frac{1}{\omega}$, the inverse of the circles' circumference, or, in our rotated coordinate system, $\frac{1}{\nu''}$. Because the distance, γ, between all rotation circles is constant, the density of circles within the plane is also constant. The density of sample points, which can be expressed as the density of circles times the density of points per circle, is therefore proportional to $\frac{1}{\omega}$. The filter ω, which is the well-known ramp filter, compensates for this varying sampling density. Because lower frequencies are sampled more densely than higher frequencies, a filter is needed to correct for this difference in sampling. Because each slice along τ is identical in sample density, the backprojection filter for non-tilted parallel-beam data is one-dimensional across projections.

A.2 Backprojection filter for tilted parallel-beam geometry

For tilted parallel-beam data ($\phi \neq 0$), Figure 3 (top) illustrates the region of frequency space sampled by a projection at angles

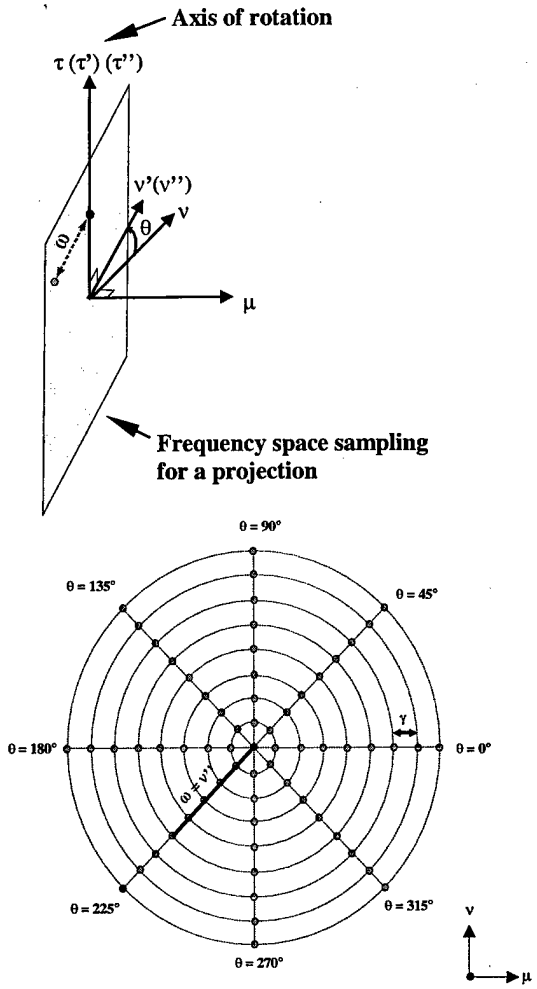

Fig. 2. (Top) Illustration of Fourier projection-slice theorem for non-tilted data. The plane indicates the frequencies sampled by a projection at angle θ. ω represents the distance between an arbitrary sample point and the τ axis. (Bottom) Frequency domain slice at a constant value of τ showing the discrete sample points at distances $\nu'' = \nu' = \omega$ from the AOR and rotated by θ. Distance γ represents the constant distance between circles of discrete sample points.

θ and ϕ. The distance ω from the axis of rotation τ to a sample point is $\omega = \sqrt{\nu''^2 + \tau''^2 \sin^2\phi}$.

Sampled frequencies correspond to discrete values of ν'', and each value of ν'' lies on a circle of sample points having a radius ω, with one sample point per angle θ. The density of points along a given circle is inversely proportional to the circles' radius, that is, proportional to

$$\frac{1}{\sqrt{\nu''^2 + \tau''^2 \sin^2\phi}}. \tag{3}$$

In contrast to non-tilted data, the distance, γ, between circles in this plane is not constant but rather depends upon ν'' and τ'' (Fig. 3, bottom). The density of circles is proportional to the reciprocal of the distance between circles, that is, proportional to

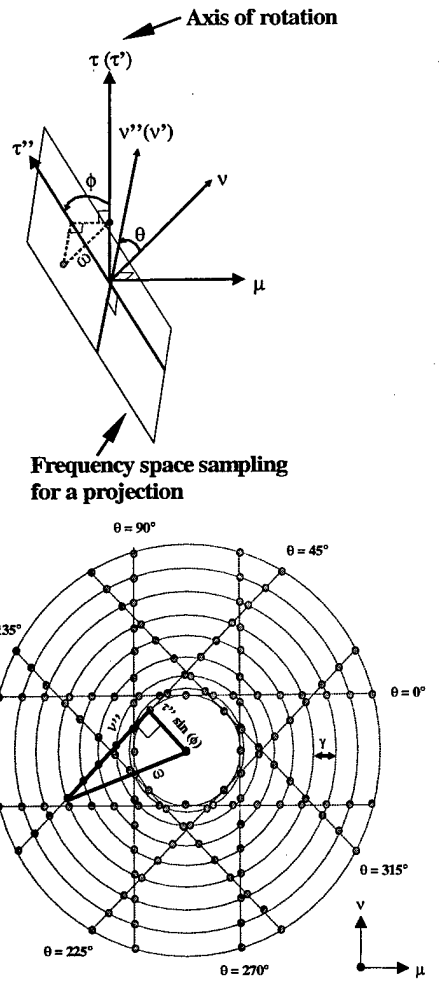

Fig. 3. (Top) Illustration of Fourier projection-slice theorem for tilted data. Plane illustrates the frequency space sampling for a projection at angles θ and ϕ. ω represents distance between arbitrary sample point and the τ axis. (Bottom) Frequency domain slice at constant value $\tau \neq 0$ built up from discrete sample points along ν'' and over rotation angles θ. Frequencies are not measured within the concentric, inner circle of radius of $\tau \sin\phi$. Unmeasured frequency region decreases as $\tau \to 0$ and becomes Figure 2 (bottom) when $\tau = 0$. Note distance ω is now a function of both ν'' and $\tau \sin\phi$. Distance γ represents the distance between circles built up from discrete sample points. Note circles are more dense near $\omega = \tau \sin\phi$ and less dense with increasing ω. For simplicity, sample points were only shown at 45° increments. Conventional, finer sampling would diminish this non-uniform density appearance within each circle.

$$\frac{d\nu''}{d\omega} = \frac{\sqrt{\nu''^2 + \tau''^2 \sin^2\phi}}{|\nu''|}. \qquad (4)$$

As ν'' increases, the distance between neighboring circles increases. These circles are more dense near $\omega = \tau'' \sin\phi$ than at higher ω. For $\omega < |\tau'' \sin\phi|$, the density of sample points within the plane is zero. For $w \geq |\tau'' \sin\phi|$, the density of sample points within the plane is the product of (3) and (4), which is $\frac{1}{|\nu''|}$.

Finally, because the spacing of sample points in the τ direction for tilted data is constant, although compressed, a third constant component, $\frac{1}{\cos\phi}$, can be included.

Multiplying these three density components yields

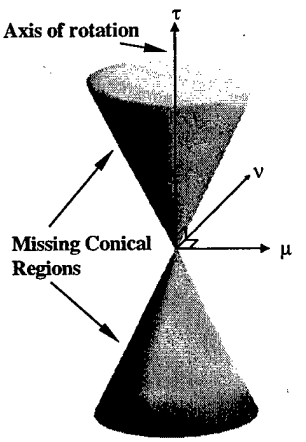

Fig. 4. Illustration of missing conical regions present in all TH-SPECT frequency space representations. Volume of missing region increases with tilt angle ϕ.

$$\frac{1}{\sqrt{\nu''^2 + \tau''^2 \sin^2\phi}} \cdot \frac{\sqrt{\nu''^2 + \tau''^2 \sin^2\phi}}{|\nu''|} \cdot \frac{1}{\cos\phi} = \frac{1}{|\nu''| \cos\phi} \qquad (5)$$

for the density of all points when $\omega \geq |\tau'' \sin\phi|$. This density is the modulation transfer function (MTF) of the ideal (no attenuation, perfect spatial resolution) tilted parallel-beam measurement. For $\omega < |\tau'' \sin\phi|$ the MTF is zero, so those frequencies cannot be recovered. These frequencies can be represented as missing conical regions whose volumes increase with tilt angle ϕ (Fig. 4).

For $\omega \geq |\tau'' \sin\phi|$, (5) indicates that the MTF can be inverted by the scaled ramp filter, $|\nu'' \cos\phi|$. This geometrical derivation is consistent with previous derivations of the backprojection filter for the tilted parallel-beam geometry [2].

B. Simulated Breast Scan

In order to compare OSEM and FBP for tilted parallel-beam breast imaging, a vertical axis of rotation (VAOR) scan was simulated using a section of the digital anthropomorphic Peter phantom [11]. This computer phantom consists of various volumetric regions in the torso (Fig. 5). For this study, only the left breast (11 cm base-to-nipple, 14 cm base diameter) containing a uniform activity concentration was scanned and no torso activity was present. The phantom was implemented on a 168x168x168 grid, voxels 0.35 cm on a side. The camera's AOR, coincided with a line from the base of the breast through the nipple (Fig. 6). The simulated VAOR scan used a 22.4 cm x 22.4 cm field-of-view (FOV) parallel-hole gamma camera, and each projection data set was acquired for 128 angular views over 360°. Each projection was 64x64 pixels and pixel size was 0.35 cm square. Projection data were simulated for 0°, 15°, 30°, and 45° tilt angles. Expected values for VAOR projection data were analytically computed based on forward projections of activity within the breast region only. Compton scattering, attenuation, and collimator and crystal spatial resolution were not modeled.

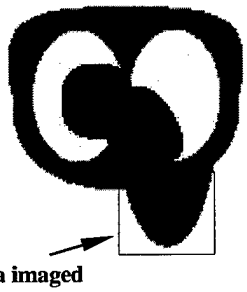

Fig. 5. Transverse view of digital anthropomorphic Peter phantom. Squared breast region indicates the subsection of phantom which was imaged.

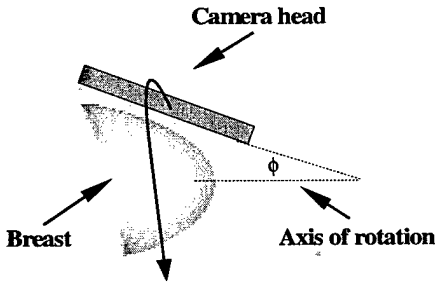

Fig. 6. Illustration of simulated breast scan. Breast represents subsection of digital anthropomorphic Peter phantom and ϕ represents angular camera tilt.

An ensemble study was generated consisting of 50 acquisitions per tilt angle and based on Poisson variation about the expected values. OSEM reconstructions were performed with the tilted geometry modeled in the photon detection probabilities, and noise and bias values were computed for 1-50 iterations (8 subsets). Reconstructed OSEM images were 32x32x32 cubic voxels each, 0.7 cm wide. Compton scattering, attenuation, and collimator and crystal spatial resolution were not modeled within the reconstruction. FBP reconstruction was similarly performed with images also 32x32x32 cubic voxels, 0.7 cm wide. FBP images were post-filtered using a 3-D Butterworth filter. Butterworth filter cut-off frequencies, the frequencies at which the gain equals 0.707, ranged from 0.1 - 1.0 cycles/pixel with frequency order equal to 10.

Noise vs. bias curves were generated for both OSEM and FBP reconstructions. Noise was computed as the standard deviation over the ensemble on a pixel-by-pixel basis. Bias was defined as $\sqrt{\sum_{i=1}^{N}(\bar{x}_i - x_i^{(t)})^2}$, where N is the number of voxels, $\bar{x}_i$ is the ith pixel value of the average image, and $x_i^{(t)}$ is the value of the ith pixel in the true phantom image.

C. Defrise Disk Phantom Scan

Mini-Defrise phantom disks (Data Spectrum Corp., Hillsborough, NC) were placed inside a fillable breast phantom (Model ECT/FL BR/A, Data Spectrum Corp., Hillsborough, NC) (Fig. 7). Data were acquired using one head of a tiltable two headed SPECT system (Vision T-22, Summit Nuclear, Twinsburg, OH) and a parallel beam low energy high resolution (LEHR) collimator (Hitachi, Tokyo, Japan) (hole length = 41.0 mm, flat to flat hexagonal hole size = 1.8 mm, septal thickness = 0.18 mm). The breast phantom contained three cold Defrise-phantom disks measuring 1.0 cm in thickness and 8.0 cm in diameter and with a 1.0 cm gap between disks. The breast phantom was filled with water having a 22.5 μCi/ml concentration of Tc-99m. The axis of the breast phantom was then aligned parallel to the camera's AOR through the nipple, and the radius of rotation (ROR) was measured perpendicular to the center of the camera and to the nipple. Projection data were acquired for tilt angles of 0°, 5°, 10°, and 15° having ROR's of 12.1 cm, 11.8 cm, 11.4 cm, and 10.5 cm respectively. The ROR decreased with greater tilt angle due to greater access to the breast. Total acquisition time was 10 seconds per angular step or 21.33 minutes over 360 degrees. Acquisition times were adjusted to compensate for radioactive decay.

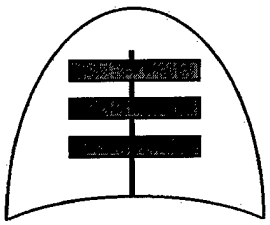

Fig. 7. Schematic of breast phantom with three mini-Defrise disks. Nipple is at top and curvature at bottom corresponds to torso shape.

OSEM (8 subsets, 3 iterations) and FBP (Butterworth filtered, cut-off = 0.5 cycles/cm, order = 10) reconstructions were performed for all tilt angles, and final images were 128x128x128 cubic voxels, 0.48 cm on a side. Iteration and filter parameters were determined from aforementioned noise vs. bias study.

D. Fillable Breast Phantom with Lesions

The fillable breast phantom (950 ml) containing two spherical lesions, 1.0 cm diameter (0.52 ml) and 0.6 cm diameter (0.11 ml) (models ECT/HOL-468/A, Data Spectrum Corp., Hillsborough, NC), was also imaged in this experiment (Fig. 8). Data were acquired using a < 13 cm x 13 cm FOV LumaGEM™ gamma camera (Gamma Medica, Inc., Northridge, CA) (hole length = 23.6 mm, flat to flat hexagonal hole size = 1.22 mm, septal thickness = 0.2 mm) as a component on a dedicated Application Specific Emission Tomograph (ASET) gantry [12] (Fig. 9). The breast phantom contained ^{99m}Tc-pertechnetate (140.6 keV) activity and water and lesions:breast activity concentration was 5.94:1. Images were acquired for 128 angular views over 360°, and each projection was 54x54 pixels, each 2.2 mm square. Total acquisition time was 20 minutes, or 9.375 seconds per angular step. Projection data were acquired for 0°, 10°, 20°, and 30° tilt angles with ROR's of 7.47 cm, 6.63 cm, 5.48 cm, and 5.48 cm respectively, measured from the camera head to the center-of-rotation point. Greater tilted angles allow for the smaller ROR's.

OSEM (8 subsets, 3 iterations) and FBP (Butterworth filtered, cut-off = 0.5 cycles/cm, order = 10) reconstructions were performed for all tilt angles, and final images were 54x54x54 cubic voxels, 0.22 cm on a side. Iteration and filter parameters were determined from aforementioned noise vs. bias study to provide

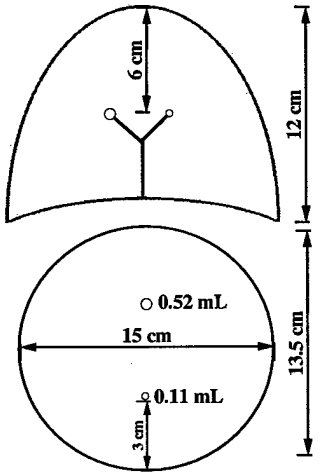

Fig. 8. Schematic of 950 ml breast phantom containing lesions. Large lesion is located at a superior medial aspect of the breast, 6 cm from nipple and 3 cm from a normal to the surface of the breast. Smaller lesion is located at an inferior medial aspect of the breast, 6 cm from nipple and 3 cm from a normal surface of the breast. (Top schematic shows relative height and lesion displacement; Bottom schematic illustrates actual lesion orientation in the breast)

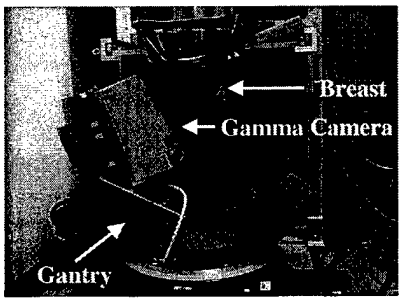

Fig. 9. Photograph of fillable breast phantom suspended over the ASET system.

similar noise levels for both methods.

For both reconstruction methods at all degrees of tilt, an elliptical, 11 pixel region-of-interest (ROI) was taken for the large lesion and a similar 121 pixel ROI was taken in the breast. Lesion contrast was calculated as $\frac{\mu_{lesion}-\mu_{breast}}{\mu_{breast}}$, and SNR as $\frac{\mu_{lesion}-\mu_{breast}}{\sigma_{breast}}$, where μ = mean and σ = standard deviation of selected ROI's.

III. Results

A. Simulated Breast Scan

Figure 10 presents noise vs. bias plots for OSEM and FBP reconstructions of the simulated breast scan. Figure 11 presents transaxial, sagittal, and coronal mid-slices (with respect to the breast reference frame) for FBP (no post-filtering), and OSEM (3 iterations) reconstruction methods at 0°, 15°, 30°, and 45°. Iteration cut-offs were chosen to provide approximately equal noise for both reconstruction methods. FBP results indicate a greater increase in backprojection artifacts with greater angular tilt. OSEM reconstructions were better able to maintain a clear, defined border around the breast, but both methods displayed some degree of axial stretching of the breast as well as inaccurate activity distribution with greater tilt. Stretching ef-

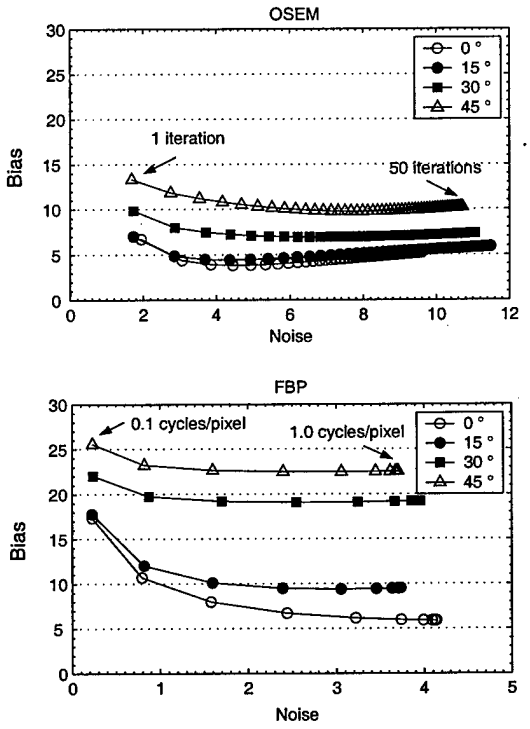

Fig. 10. Noise vs. bias plots for OSEM (top) and FBP(bottom) reconstructions of simulated breast scan at 0°, 15°, 30°, and 45° tilt. OSEM data points correspond to iterations 1 through 50 in increments of one iteration from left to right. FBP data points indicate Butterworth filter cutoffs (1.0 to 0.1 cycles/pixel in increments of 0.1 cycles/pixel from right to left, where furthest right point indicates no post-filtering). OSEM yielded the lower bias for similar noise values.

fects were not found transaxially, however, due to complete frequency sampling of the $\tau = 0$ plane (Fig. 3). This is consistent with tilted cone-beam reconstruction [13], [14], where distortions were most pronounced along the direction parallel to the rotation axis but not along the transverse direction. Ideally, the breast would be fully angularly sampled to satisfy the Orlov condition, and hence reduce currently observed elongation and object distortion artifacts [1], [4].

FBP noise vs. bias plots indicate greater bias with tilt angle compared to OSEM reconstructions (Fig. 10). A 50% increase in bias was noted between FBP 0° and 15° recontructions, while only a 15% increase in bias was noted between OSEM 0° and 15° reconstructions, compared at similar noise levels. Butterworth filtering tended to offer the best compromise between noise and bias for FBP reconstructions, specifically at a 0.3 cycles/pixel cutoff. Three iterations displayed the best noise/bias trade-off for OSEM 0°, 15°, and 30° data and four iterations were found optimal for 45° data. OSEM reconstructions displayed the lower overall bias.

B. Defrise Disk Phantom Scan

Figure 12 displays reconstructions of mini-Defrise phantom disks placed inside a fillable breast phantom. The resulting profiles indicate a bowing effect slightly visible at 10° tilt, and more clearly visible at 15° tilt. OSEM Defrise disk contrast was significantly better at greater tilt angles compared to FBP

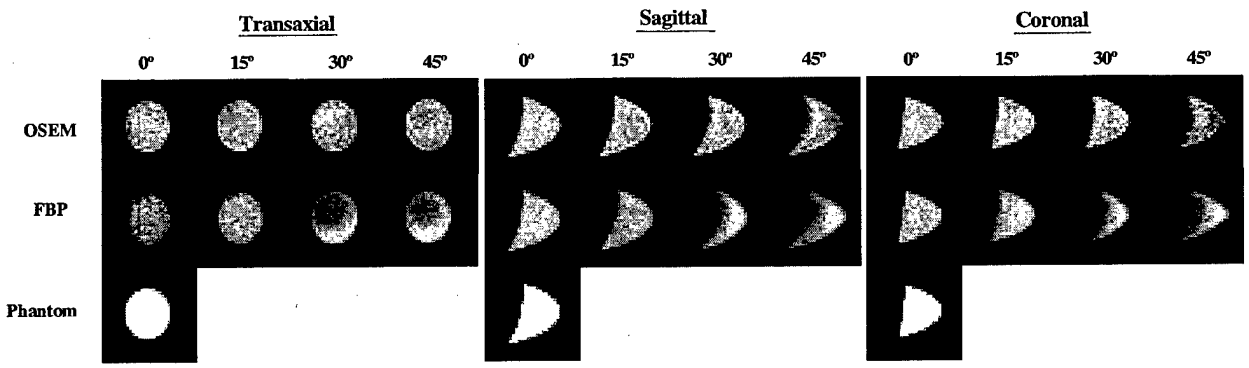

Fig. 11. Transaxial, coronal, and sagittal (with respect to the breast reference frame) OSEM and FBP reconstruction slices for simulated breast scan. Slices were taken for 0°, 15°, 30°, and 45° tilt and corresponding truth phantom slices located at bottom.

TABLE I
CONTRAST AND SNR VALUES OF LARGE LESION FOR OSEM AND FBP RECONSTRUCTIONS.

	SNR	Contrast	ROR (cm)
OSEM			
0°	9.98	2.65	7.47
10°	13.43	3.84	6.43
20°	12.23	2.82	5.48
30°	12.85	3.57	5.48
FBP			
0°	5.57	2.26	7.47
10°	6.39	2.13	6.43
20°	6.59	2.75	5.48
30°	9.10	3.25	5.48

results. OSEM reconstruction sets displayed a one pixel (0.48 cm, 3.8%) increase in breast length at 15° tilt, measured from the nipple to the anterior wall. FBP profiles indicated a two pixel (0.98 cm, 7.6%) increase in breast length. All profiles drawn axially across the right-center of the breast indicate an increase in counts toward the nipple due to attenuating effects of the Defrise disk phantom within the breast.

C. Fillable Breast Phantom with Lesions

Table I presents contrast and SNR values for reconstructions of the fillable breast phantom containing lesions (Fig. 13). OSEM reconstructions showed greater SNR and contrast values at all tilt angles. Because camera tilt allows greater access to the breast and in turn decreases the effective ROR, overall contrast and SNR values generally increased with tilt angle, confirming the effectiveness which can be achieved with TH-SPECT and dedicated compact gamma cameras.

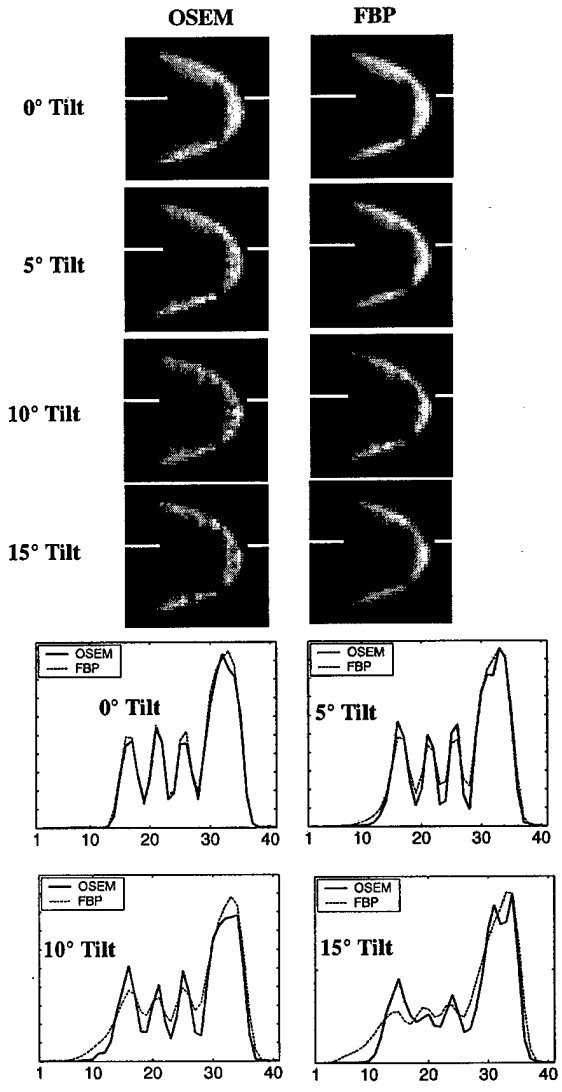

Fig. 12. Sagittal view OSEM and FBP reconstructions of mini-Defrise phantom combined with fillable breast phantom and corresponding profiles. Profile markers are drawn axially across left-center of breast phantom.

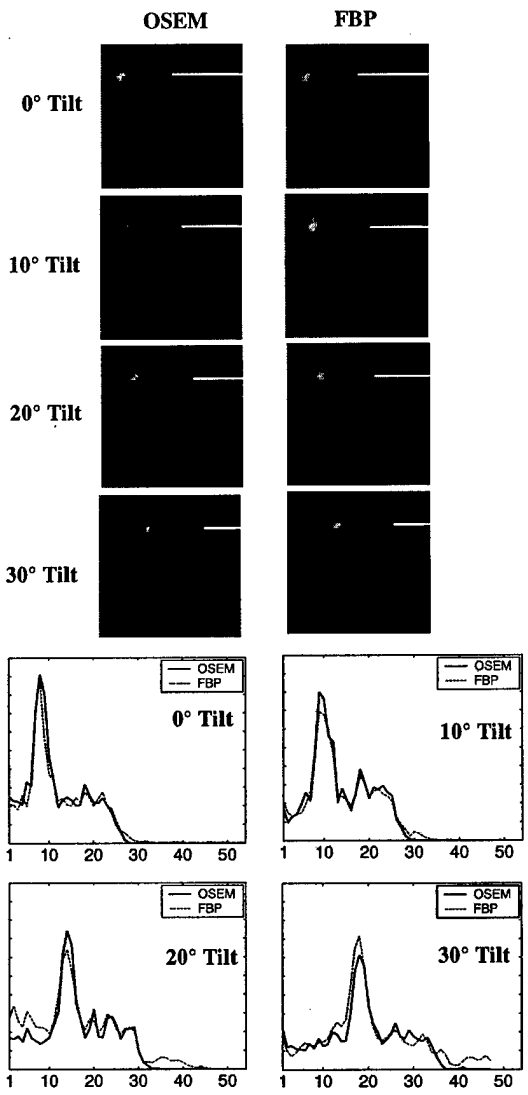

Fig. 13. Sagittal view OSEM and FBP reconstructions of anthropomorphic torso phantom combined with fillable breast phantom containing lesions. Profile markers are drawn axially across left-center of breast phantom.

IV. Discussion and Conclusion

This paper has presented a geometric derivation of the ramp filter for tilted parallel-beam geometries. FBP simulation results indicated a greater increase in artifacts with increasing tilt, as compared with iterative reconstruction, which better maintained overall breast shape. Simulation-based noise vs. bias studies indicated near-optimal iteration and cut-off parameters for each method, and showed less bias at a given noise for OSEM as compared to FBP. Phantom studies demonstrated consistently higher SNR and contrast values for OSEM reconstructions at all tilt angles.

TH-SPECT data do not sufficiently sample the Orlov sphere and therefore artifacts are present in all TH-SPECT reconstructions. The effect of these insufficiencies can be examined in frequency space the as missing conical regions shown in Figure 4. This "missing cone" problem has been investigated in a variety of different 3-D imaging systems with limited view angles [2], [15], [16], [17]. If frequency components within the missing cone and especially along the τ axis are assumed to be zero, the reconstructed mean densities of all planes perpendicular to z will be equal. This has the effect of producing unwanted activity in areas where activity should be zero or near-zero. These activity distortions are observed in FBP techniques as streak artifacts (Fig. 11) along the axis of rotation. Due to complete sampling of the $\tau = 0$ plane, transverse slices do not exhibit streak artifacts, although in-plane distortions are present.

The quality of TH-SPECT reconstructions clearly degrades with tilt angle, specifically due to the volumetric increase in null space. The fraction of null space to total frequency volume is given as

$$\frac{Null\ space}{Total\ volume} = \sin\phi. \tag{6}$$

With 30° tilt, only 13.4% of frequency space accounts for missing data. With 60° tilt, however, half of the frequency data is missing. This non-linear increase in unsampled volume indicates tilt angles over 30° may not be useful for breast SPECT.

The conjugate views for non-tilted projections exist, and therefore θ need only be sampled from 0 to π. For tilted projections, however, the conjugate view does not exist and θ should be sampled from 0 to 2π. This is illustrated in Figure 3 (bottom) as rotation from 0° to 180° degrees does not even fully sample the frequency space region outside the circle of radius $\tau'' \sin\phi$.

Herein we have investigated tilted orbits in which the camera center moves along a circle, elucidating the nature of the incomplete sampling provided by these orbits and the effectiveness of FBP and OSEM in utilizing this incomplete data. In other work, we proposed circle-plus-arc [1], [4] and more elaborate orbits that do provide complete sampling of an isolated breast, and we have developed a SPECT system capable of implementing such orbits [12].

V. Acknowledgments

The authors would like to thank Duke Health Systems for the use of the gamma camera, Nancy Jaszczak and Data Spectrum Corp. for use of phantoms, and Kim Greer for technical assistance with data collection.

References

[1] B.C. Pieper, J.E. Bowsher, M.P. Tornai, J. Peter, K. Greer, R.J. Jaszczak, "Breast tumor imaging using a tiltable head SPECT camera," *IEEE Trans. Nucl. Sci.*, vol. 48, no.4, pp 1477-1482, 2001.

[2] M. Radermacher, "Three-dimensional reconstruction of single particles from random and nonrandom tilt series," *J. Electron Microscopy Technqiue*, vol. 9. pp 359-394, 1988.

[3] S.S. Orlov, "Theory of three dimensional reconstruction," *Sov. Phys. Crystallogr.*, vol. 20, no. 3, pp. 312 314, 1975.

[4] S.D. Metzler, J.E. Bowsher, M.P. Tornai, B.C. Pieper, J. Peter, and R.J. Jaszczak, "SPECT breast imaging combining horizontal and vertical axes of rotation," *IEEE Trans. Nucl. Sci.*, vol. 49, no. 1, pp 31-36, 2002.

[5] A.C. Kak, M. Slaney, *Principles of Computerized Tomographic Imaging*, Ch. 9, pp. 49-112, IEEE,Inc., New York: IEEE Press, 1988.

[6] R.N. Bracewell, A.C. Riddle, "Inversion of fan-beam scans in radio astronomy," *Astrophys. J.*, vol. 150, pp. 427-434, Nov. 1967.

[7] G.N. Ramachandran, A.V. Lakshminarayanan, "Three dimensional reconstructions from radiographs and electron micrographs: Application of convolution transforms," *Proc. Nat. Acad. Sci.*, vol. 68, pp. 2236-2240, 1971.

[8] A. Rosenfeld, A.C. Kak, *Digital Picture Processing*, 2nd ed. New York, NY: Academic Press, 1982.

[9] G.T. Herman, "Emission Computed Tomography," in *Image Reconstruction from Projections: the Fundamentals of Computerized Tomography,* T.F. Budinger, G.T. Gullberg, and R.H. Huesman, pp. 147-246, New York: Academic Press, 1980.

[10] J.C. Russ, *The Image Processing Handbook,* Ch. 5, pp. 305-370, CRC, Boca Raton, Fl., 1999.

[11] J. Peter, M. P. Tornai, R. J. Jaszczak, "Analytical versus voxelized phantom representation for monte carlo simulation in radiological imaging," *IEEE Trans. Med. Imag.*, vol. MI-19, no. 5, pp. 556 564, 2000.

[12] M.P. Tornai, J.E. Bowsher, C.N. Archer, J. Peter, L.R. MacDonald, B.E. Patt, J.S. Iwanczyk, R.J. Jaszczak, and R.E. Coleman, "Dedicated breast imaging with an ASET: Application Specific Emission Tomograph," *J. Nucl. Med.*, vol. 42, no.5, p. 97P, 2001.

[13] J. Li, R.J. Jaszczak, K.L. Greer, R.E. Coleman, Z.J. Cao, B.M.W. Tsui, "Direct cone beam SPECT reconstruction with camera tilt," *Phys. Med. Biol.*, 38:241-258, 1993.

[14] P. Grangeat, P. Masson, P. Melennec, P. Sire, "Evaluation of the 3D Radon transform algorithm for cone beam reconstruction," *Proc. SPIE* 1445, pp 320-31, 1991.

[15] J. Frank, *Electron Tomography,* Plenum Press, New York, 1992.

[16] F. Natterer, *The Mathematics of Computerized Tomography,* John Wiley & Sons Ltd, 1986.

[17] M.Y. Chiu, H.H. Barrett, R.G. Simpson, C. Chou, J.W. Arendt, G.R. Gindi, "Three-dimensional radiographic imaging with a restricted view angle," *J. Opt. Soc. Am.*, vol. 68, no.10, pp 1323-1333, October 1979.

Breast Tumor Imaging Using a Tiltable Head SPECT Camera*

Brett C. Pieper[1,2], *Student Member, IEEE*, James E. Bowsher[1], *Member, IEEE*, Martin P. Tornai[1], *Member, IEEE*, Jörg Peter[1], *Member, IEEE*, Kim Greer[1], Ronald J. Jaszczak[1,2], *Fellow, IEEE*
[1]*Duke University Medical Center, Department of Radiology, Durham, NC 27710, USA*
[2]*Department of Biomedical Engineering, Duke University, Durham, NC 27710, USA*

Abstract

As a test bed for dedicated breast SPECT cameras that are under development, a general purpose SPECT system with two tiltable heads was used to image fillable breast and torso phantoms containing multiple lesions. Breast, liver, and myocardial activity were included in order to simulate direct contamination and Compton scattering expected in clinical scans. The TH–SPECT data were reconstructed using an OS–EM algorithm which accounted for the tilted geometry. High count planar images were acquired for comparison with tilted–head SPECT (TH–SPECT). In order to characterize axial blurring effects inherent with TH–SPECT reconstructions, two cylindrical disk Defrise phantoms, one large Defrise phantom and one mini–Defrise phantom placed inside the fillable breast phantom, were imaged at various tilt angles. Results indicate an increase in axial blurring with greater tilt angle. Reconstructions of the combined fillable breast and torso phantoms containing two 1.15 ml lesions, one centered axially and one proximal to the anterior chest wall within the breast, were most clearly visible in the 30° reconstructed TH–SPECT images, providing lesion SNR and contrast improvements of nearly three times compared to the high–count planar images

I. INTRODUCTION

For breast cancer imaging using conventional Single Photon Emission Computed Tomography (SPECT) systems, the gamma camera's axis of rotation is parallel to the patient table – a horizontal axis of rotation (HAOR). This geometry decreases breast signals due to torso attenuation and, more importantly, requires a large radius of rotation which yields poor results for SPECT breast imaging [1].

Previous work indicates breast cancer imaging can be improved by using a vertical axis of rotation (VAOR) [1], [2]. In this work, we expand upon previous VAOR breast imaging by using tiltable gamma cameras. By tilting the camera off axis with respect to the nipple–to–anterior chest axis through the breast, improved imaging of lesions near the chest wall and a reduced radius of rotation (ROR) can be achieved. This paper investigates tilted VAOR breast imaging (Fig. 1) by simulating a dedicated VAOR system using a HAOR SPECT system with tiltable gamma cameras.

One major concern with Tiltable–Head SPECT (TH–SPECT) imaging is insufficient angular sampling. The completeness of reconstructions using TH–SPECT is bound by Orlov sphere conditions [3]. In order to satisfy these conditions, the image space must be sampled over a great circle or equatorial orbit. By tilting the camera heads off axis, this primary requirement is not met (Fig. 2), and thus there is the potential for artifacts in the reconstructed images. This is also an issue, in general, with slant–hole collimators and rotating slant–hole collimators [4].

Another concern with TH–SPECT imaging is background interference from myocardium, liver, and body tissue that is expected clinically with the use of Tc–99m labeled tracers. By tilting the camera heads off axis, heart

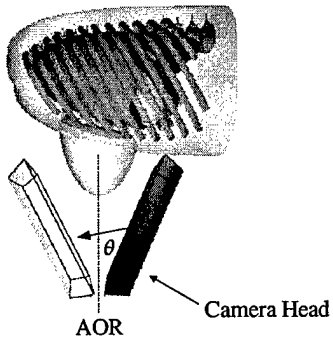

Figure 1: Schematic of dedicated breast VAOR system.

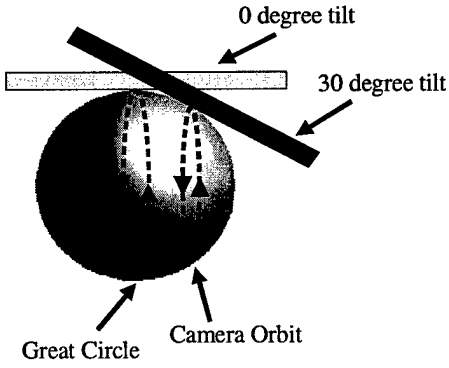

Figure 2: Sphere showing an equatorial camera orbit and an orbit where the camera head is tilted. The camera is normal and tangentral to the sphere at all projection views.

* Manuscript received November 12, 2000. This work was funded by PHS grants R01–CA76006 and R01–CA33541 from the National Institutes of Health, grant RG–99–0305 from the Whitaker Foundation, and grant DE–FG02–96ER62150 from the Department of Energy.

and liver activity are introduced into the camera's field of view (FOV) at some projections, potentially contaminating TH–SPECT reconstructions.

The following measured results indicate, however, that myocardium, liver, and tissue background interference do not markedly affect breast lesion contrast or signal–to–noise ratio (SNR) values. Furthermore, tilted head acquisitions can be successfully reconstructed, and although axial distortions are present and significantly increase at greater tilt angles, excellent SNR and contrast values are obtained for lesions, including those near the chest wall.

II. MATERIALS AND METHODS

All data were acquired using a tiltable two–headed SPECT system (Vision T–22, Summit Nuclear, Twinsburg, OH) (Fig. 5). Only one head was used to obtain data during this study. A parallel beam low–energy high–resolution (LEHR) collimator (Hitachi) was used in all experiments. Collimator hole length was 41.0 mm, hexagonal hole size was 1.8 mm, flat–to–flat and septal thickness was 0.18 mm. All images were reconstructed by OS–EM (5 iterations, 8 subsets), with the tilted geometry modeled in the photon detection probabilities. Compton scattering, attenuation, and collimator and crystal spatial resolution were not modeled.

A. Defrise Disk Phantom

A Defrise disk phantom (Fig. 3) (Data Spectrum Corp., Hillsborough, NC) was utilized in the first experiment. This phantom consisted of a cylinder containing six acrylic disks placed 1.5 cm apart. The acrylic disks had a thickness of 1.2 cm and a diameter of 18.9 cm. Five emission disks were then formed by adding 16.6 mCi of Tc–99m and water to the cylinder, each hot disk having a uniform concentration of 4.1 μCi/ml. The phantom was then placed parallel to the camera's axis of rotation (AOR) with a radius of rotation (ROR) of 11.5 cm, measured from the center of the camera to the Defirse disk phantom's long axis, perpendicular to the camera's AOR (Fig. 3). Projection data were taken for 0°, 15°, 30°, 45°, and 60° tilt angles. Each projection data set was acquired for 128 angular views over 360°, and each projection was 128x128 pixels and pixel size was 0.48 cm square. Total acquisition time was 7 seconds per angular step for a total time of 15 minutes. Subsequent acquisition times were increased to compensate for radioactive decay.

B. Breast Phantom with Mini–Disk Phantom

In order to characterize axial blurring within the breast geometry, custom mini–Defrise phantom disks (Data Spectrum Corp., Hillsborough, NC) were placed inside a custom fillable breast phantom (Data Spectrum Corp., Hillsborough, NC) (Fig. 4). By filling the breast phantom with water having a 22.5 μCi/mL concentration of Tc–99m, three cold disks measuring 1.0 cm in thickness and 8.0 cm in diameter and two hot disks measuring 1.0 cm and 8.0 cm in diameter were formed. The axis of the breast phantom was then placed parallel to the camera's AOR and the radius of rotation was measured from the nipple to the center of the camera, perpendicular to the camera's AOR. Because axial blurring becomes extremely noticeable at larger tilt angles (> 15°), projection data were taken for angles of 0°, 5°, 10°, and 15° having ROR's of 12.1 cm, 11.8 cm, 11.6 cm, and 10.9 cm respectively. The ROR was decreased with greater tilt angle due to greater access to the breast. Potentially smaller ROR's would be possible with dedicated small area breast imaging systems. Total acquisition time was 10 seconds per angular step or 21.33 minutes. Subsequent acquisition times were increased to compensate for radioactive decay.

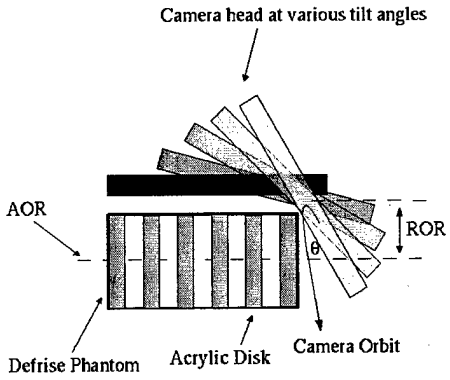

Figure 3: Schematic of the Defrise phantom with camera head at 0°, 15°, 30°, 45°, and 60° tilt angles. Curved arrow illustrates camera orbit out of page about the AOR.

Figure 4: Photograph of the custom breast phantom with three mini–Defrise disks 8.0 cm in diameter and 1.0 cm thick, separated by a 1.0 cm gap and aligned along the breast axis. Nipple is at right, and curvature at left corresponds with torso shape.

C. Anthropomorphic Torso Phantom and Breast Phantom with Lesions

An anthropomorphic torso phantom (Model ECT/TOR/P, Data Spectrum Corp., Hillsborough, NC)

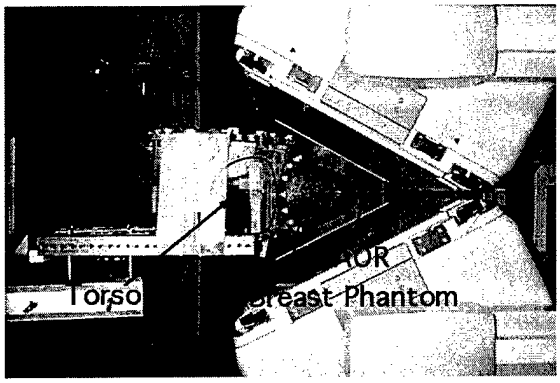

Figure 5: Photograph of anthropomorphic torso and breast phantoms with dual tilted heads on the SPECT camera.

combined with the fillable breast phantom was imaged in this experiment (Fig. 5) to simulate the expected emission contamination from the myocardium and liver to the specific breast imaging task. The craniocaudal axis of the torso phantom was perpendicular to the camera's axis of rotation, thus necessitating the tilted camera heads and allowing for close proximity imaging of the breast phantom. Two 1.3 cm diameter lesions (1.15 ml) with Tc–99m concentration of 11.1 μCi/ml were suspended inside the left breast. One lesion was placed axially in the center of the breast, 5.1 cm from the nipple. The second lesion was located 2.2 cm anterior to the chest wall and positioned 3.0 cm towards the medial–superior side of the breast. A third 0.9 cm diameter lesion (0.38 ml) with a concentration of 11.1 μCi/ml was placed outside the breast on the chest wall to represent axillary tumor growth. The breast phantom had a uniform concentration of 1.5 μCi/ml. In order simulate contamination effects due to direct superposition of myocardial activity on the breast at some projection views and also Compton scattering expected in clinical scans, the tumor and breast were imaged with additional liver and myocardium activity. The lesion:liver:myocardium:breast–background ratio was 7.4:12.5:12.5:1, giving the liver and heart a Tc–99m concentration of 18.7 μCi/ml.

Projection data were acquired for 0°, 15°, 30°, and 45° tilt angles with ROR's of 18.1 cm, 10.5 cm, 9.4 cm, and 5.9 cm respectively, measured as previously described. The images were acquired for 128 angular views over 360°, and each projection was 128x128 pixels and pixel size was 0.48 cm square. Total acquisition time was 32 minutes, or 15 seconds per angular step and subsequent acquisition times were increased to compensate for radioactive decay.

Because planar scintimammography is gaining acceptance as an effective way to identify breast lesions greater than 1 cm in diameter [5], a planar scintimammography image (craniocaudal view) was made for comparison. Breast, liver, and myocardium background radiation were present, with the same activity concentration as for TH–SPECT, and the total acquisition time was 5 minutes.

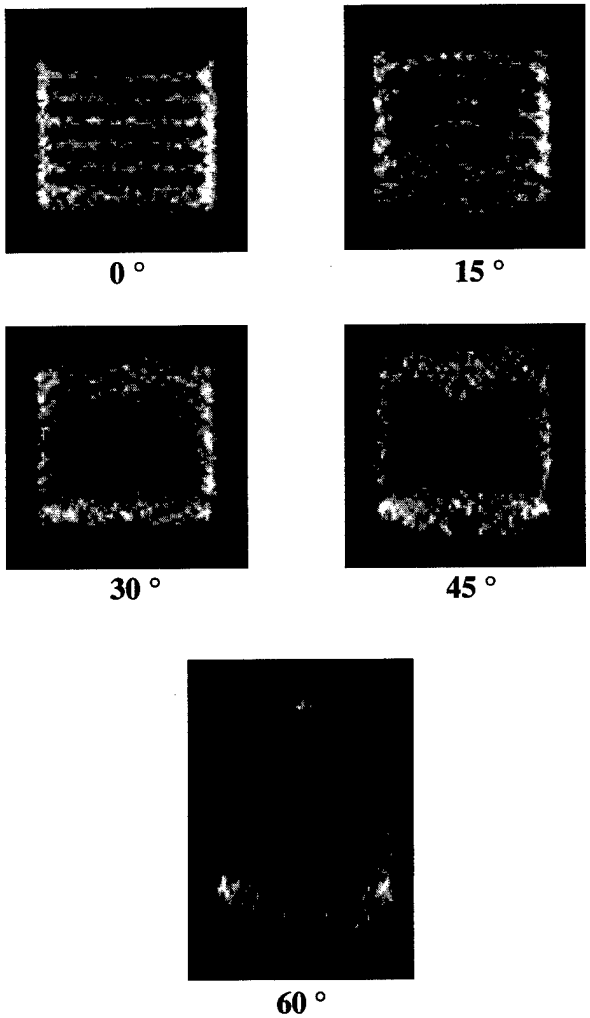

Figure 6: Single slice sagittal views of OS–EM reconstructed Defrise phantom images at indicated tilt angles.

III. RESULTS

A. Degradative Angular Sampling Effects

Single slice sagittal views of the reconstructed Defrise phantom images at 0°, 15°, 30°, 45°, and 60° are presented in Figure 6. For the reconstructed sagittal slices, each disk should be regular "bar" shape (Fig. 6., left, top), but as the tilt angle is increased there is a clear bowing effect in the axial direction which corroborates the results in [6]. The disks are almost unrecognizable in the 30°–60° tilts.

Figure 7 compares the results of the mini–Defrise phantom inserted into the fillable breast phantom. Results from the larger Defrise phantom indicated extreme axial blurring for tilt angles greater than 15°. This experiment investigated smaller tilt angles to evaluate the effects of incomplete sampling with small tilt angles, and also to attempt to minimize the blurring effect but still maximize chest wall imaging without additional orbits to complete the

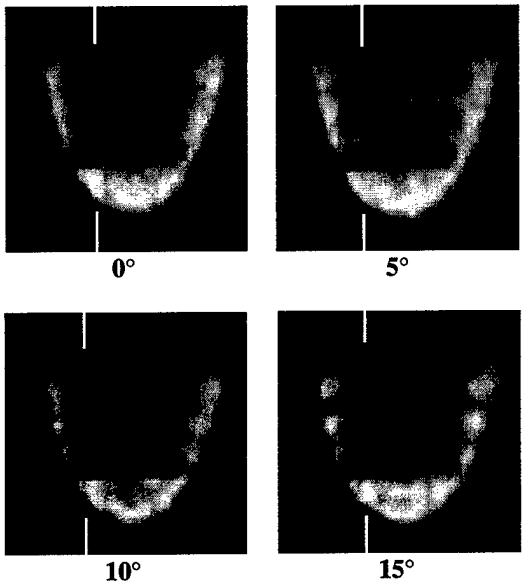

Figure 7: Single slice sagittal view OS–EM reconstructions of mini–Defrise phantom combined with fillable breast phantom at indicated angles. Profile markers are drawn axially across left–center of breast phantom.

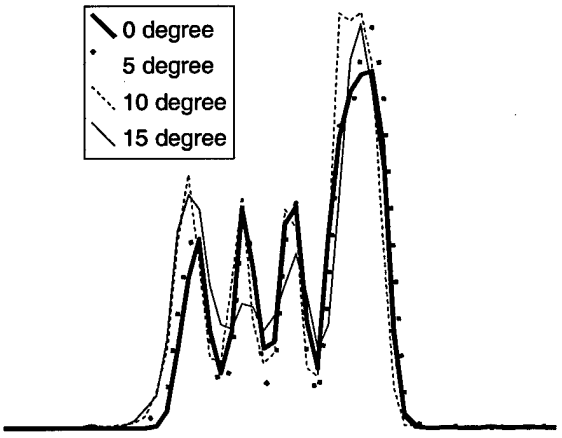

Figure 8: Profiles drawn across single slice sagittal views of mini–Defrise phantom (Fig. 7). Left corresponds to bottom portion of the images shown in Figure 7. Camera head was tilted away from chest wall. Note increase in breast's axial length with greater tilt angle.

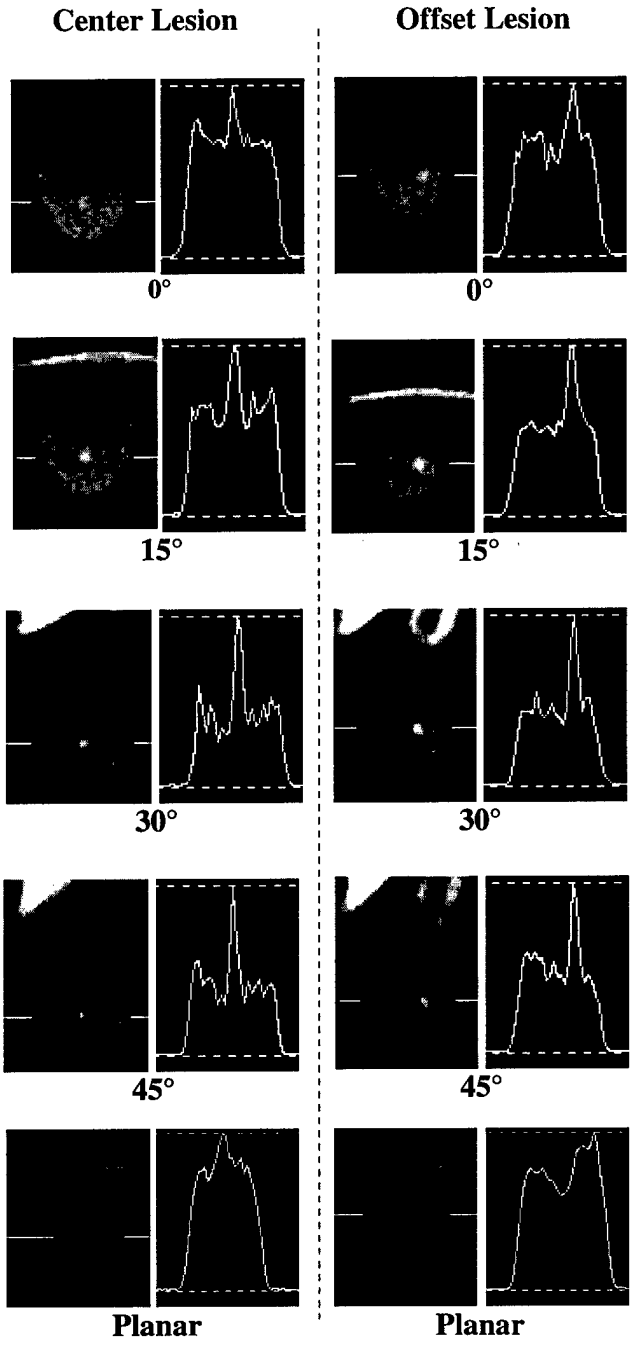

Figure 9: Sagittal view reconstructions of fillable breast phantom attached to anthropomorphic torso phantom containing two hot lesions (one lesion axially centered, one lesion anterior to the chest wall and positioned towards the medial–superior side of the breast) at 0°, 15°, 30°, and 45° tilt angles as well as conventional high–count planar images. Profiles for each lesion are also shown. The cold spot directly behind the central lesion is the acrylic support used to hold lesion in place and the cold gap between the breast and torso represents phantom chest wall.

Table 1

SNR and contrast values for center lesion and offset lesion at 0°, 15°, 30°, and 45° tilt angles as well as a conventional high–count planar image (craniocaudal view).

	SNR $[(\mu_{lesion} - \mu_{breast})/\sigma_{breast}]$	Contrast $[(\mu_{lesion} - \mu_{breast})/\mu_{breast}]$	ROR (cm)
Center lesion			
Planar	2.10	0.20	18.1
0°	2.09	0.25	18.1
15°	3.56	0.49	10.5
30°	4.89	0.59	9.4
45°	5.15	0.59	5.9
Offset lesion			
Planar	2.04	0.20	18.1
0°	2.13	0.24	18.1
15°	3.74	0.51	10.5
30°	6.32	0.63	9.4
45°	5.16	0.49	5.9

data. A bowing effect similar to that seen in Figure 6 is clear in these reconstructions, although not as pronounced.

Profiles drawn axially across the left–center of the breast (Fig. 8) indicate an increase in counts towards the nipple due to the attenuating effects of the defrise phantom within the breast. The profiles also show a definite axial "stretching" effect, as the 15° image is roughly 0.5 cm longer than the 0° image. This result indicates that visualization of axially juxtaposed tumors or shell–like tumors may be difficult to discern.

B. Lesion Imaging with Various Tilt Angles

Reconstructed sagittal views of the fillable breast phantom containing two hot lesions combined with the anthropomorphic torso phantom are presented in Figure 9 with corresponding profiles at the indicated locations. Background heart, liver and torso contamination were present, and all profiles were drawn across the center of the lesions. Table 1 compares the SNR and contrast values for each lesion and tilt angle. Figure 9 clearly shows an increase in both contrast and SNR as tilt angle is increased from 0° to 30°. Tilt angles beyond 30° do not significantly improve either contrast or SNR values.

The third lesion, attached to the anthropomorphic torso phantom anterior to the chest wall and superior to the left breast, was also reconstructed. Although not shown, the lesion is clearly visible in all reconstructions.

IV. DISCUSSION AND CONCLUSIONS

Because of insufficient sampling, axial blurring is evident in all TH–SPECT reconstructions. As shown with

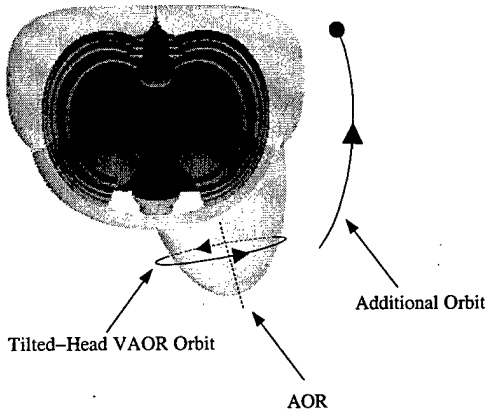

Figure 10: Transverse view of phantom illustrating TH–SPECT acquisition as well as an additional HAOR orbit to gather insufficiently sampled data.

the larger Defrise phantom, large tilt angles (45° and 60°) yield extremely distorted images. Because the ROR can be decreased as tilt angle is increased, it is important to find an acceptable combination between the two, specifically one which minimizes axial blurring effects while still maximizing SNR and contrast values. Trade–offs between higher resolution parallel hole collimators versus higher sensitivity collimators should be considered. The use of non–parallel hole collimators should also be considered in this application since these geometries could potentially help complete undersampled regions of the Orlov sphere [7].

As Figure 9 shows, larger tilt angles can "stretch" the breast axially. This stretching phenomena also affects the lesion, and can potentially blur together axially offset lesions or distort shell–like lesions. This phenomena has very little effect, however, on the 15° degree reconstruction. Compared to the 0° reconstruction which has no distortions, SNR and contrast values between the two are significantly different, providing lesion SNR and contrast improvements of up to two times for the center lesion (Table 1). Although 30° and 45° tilt reconstructions have even better SNR and contrast values, distortions of the breast are much more evident, compared to the smaller tilt angles.

As Table 1 indicates, effective radius of rotation significantly decreases as tilt angle is increased. Although the 45° radius of rotation was almost half that of the 30°, extreme insufficient sampling as well as attenuation prevented further contrast and SNR improvements. Dramatic decreases in ROR due to increasing tilt angle could not, however, be achieved using a small–area dedicated breast SPECT system, although results indicate SNR and contrast values should improve with any reduction of ROR. In addition to viewing lesions near the torso–breast interface, TH–SPECT reconstructions may considerably improve SNR and contrast values even for lesions within the breast, presumably by allowing for a reduced ROR. Localization of the lesion, however, may be difficult with the present artifacts.

The blurring and distortion artifacts become more apparent with greater axial non–uniformity in the breast, as

shown in Figure 7 with the mini–Defrise phantom. The 15° tilt reconstruction of the mini–Defrise phantom inside the fillable breast phantom highlights a definite bowing effect. These results indicate that artifacts will be more present when objects are axially aligned and imaged with a TH–SPECT technique. This bowing effect is not visualized in Figure 9 reconstructions simply due to the uniformity of breast tissue and spherical lesions. Non–uniform breast lesions, such as distorted or shell–like tumors, may result in further image degradation even at small angular tilts. Although dedicated breast SPECT systems under development may also suffer from the artifacts illustrated in this study, those systems may further provide SNR and contrast improvements due to reduced ROR's.

When the reconstruction was limited to the breast only, essentially eliminating background interference from the FOV, a cupping artifact [8] was present. This cupping artifact is an artificial increase in activity near the edge of the FOV. By reconstructing the entire image space (heart and liver interference included), this artifact was eliminated [8]. It remains to be seen if small–area dedicated breast SPECT systems will suffer from these limitations and if reconstructed images from a small–area camera contain the cupping artifact.

Possible modifications can be made to the TH–SPECT geometry to account for insufficient sampling and to reduce, if not eliminate, axial blurring artifacts. Because Orlov Sphere requirements are not met with any degree of camera tilt [3], an additional orbit is required to satisfy these conditions for fully quantitative SPECT imaging [9]. Figure 10 introduces one such additional orbit. If TH–SPECT VAOR data is collected and combined with an incomplete HAOR orbit [9], Orlov Sphere requirements should be met and blurring due to insufficient axial sampling should be eliminated. This short arc–orbit (ranging from 10° to 90° depending upon tilt angle) needs only to gather enough data to fully sample the breast, as accurate heart and liver reconstruction may not be necessary.

V. AKNOWLEDGMENTS

The authors of this paper would like to thank Duke Medical Center for the use of the gamma camera and Nancy Jaszczak and Data Spectrum Corp. for use of phantoms.

VI. REFERENCES

[1] H. Wang, C. Scarfone, K. L. Greer, R. E. Coleman, and R. J. Jaszczak, "Prone breast tumor imaging using vertical axis–of–rotation (VAOR) SPECT systems: an initial study," *IEEE Trans. Nucl. Sci.* NS44(3):1271–1276. 1997.

[2] M. P. Tornai, B. C. Pieper, J. E. Bowsher, and R. J. Jaszczak, "Effects of pinhole material and aperture size on lesion contrast and SNR in breast SPECT," *Submitted to IEEE Nuclear Science Symposium and Medical Imaging Conference, (Lyon, France).* 2000.

[3] S.S. Orlov, "Theory of three dimensional reconstruction," *Kristallografiya*, 20, 511–515 (May–June 1975).

[4] D.E. Wessell, "Rotating slant–hole single–photon emission–computed tomography," *Med. Phys.*, vol. 27(7), pp. 1697. 2000.

[5] I. Khalkali, J. A. Cutrone, I. G. Mena, L. E. Diggles, R. J. Venegas, H. I. Vargas, B. L. Jackson, S. Khalkali, J. F. Moss, and S. R. Klein, "Scintimammography: the complementary role of Tc–99m sestamibi prone breast imaging for the diagnosis of breast carcinoma," *Radiology,* vol. 336, pp. 1784–1789, 1995.

[6] C.D. Stone, M. F. Smith, K. L. Greer, and R.J. Jaszczak, "A combined half–cone beam and parallel hole collimation," *IEEE Trans. Nucl. Sci.,* vol. 45(3), pp. 1219–1224. 1998.

[7] J. Li, R. J. Jaszczak, K. L. Greer, R. E. Coleman, Z. Cao, and B. M. W. Tsui, "Direct cone beam SPECT reconstruction with camera tilt," *Phys. Med. Biol.,* vol. 38, pp. 241–258, 1993.

[8] M. A. King, D. Luo, S.T. Dahlberg, and B. J. Villegas, "Transmission imaging of large attenuators using a slant hole collimator on a three–headed SPECT system," *Med. Phys.*, vol 23(3), pp. 263–271. 1996.

[9] S. Metzler, J. E. Bowsher, M. P. Tornai, B. C. Pieper, and R. J. Jaszczak. "SPECT breast imaging combing horizontal and vertical axes of rotation," *Submitted to IEEE Nuclear Science Symposium and Medical Imaging Conference, (Lyon, France).* 2000.